Major Article

Omicron BA.1 and BA.2 sub-lineages show reduced pathogenicity and transmission potential than the early SARS-CoV-2 D614G variant in Syrian hamsters

Wen Su[1§], Ka Tim Choy[1§], Haogao Gu[1], Sin Fun Sia[1], Ka Man Cheng[1], Sarea Islam Nuha Nizami[1], Pavithra Krishnan[1], Yuet Mai Ng[1], Lydia Dai Jia Chang[1], Yingzhi Liu[1], Samuel MS Cheng[1], Malik Peiris[1], Leo LM Poon[1], John M Nicholls[2], Hui-Ling Yen[1]*

[1] School of Public Health, [2] Department of Pathology, Li Ka Shing Faculty of Medicine, The University of Hong Kong, Hong Kong SAR, China

[§]These authors contributed equally. *Correspondence: HL Yen (hyen@hku.hk).

Running title: Omicron BA.1 and BA.2 in Syrian hamsters

Notes:

(1) The authors have no commercial or other association that might pose a conflict of interest.

(2) This study was supported by National Institute of Allergy and Infectious Diseases of the National Institutes of Health, USA (U01AI151810 and 75N93021C00016), Research Grant Council Theme-based Research Schemes, Hong Kong SAR, China (T11-712/19-N and T11-705/21-N).

(3) Correspondence: HL Yen (hyen@hku.hk).

ACCEPTED MANUSCRIPT

© The Author(s) 2022. Published by Oxford University Press on behalf of Infectious Diseases Society of America. All rights reserved. For permissions, please e-mail: journals.permissions@oup.com This article is published and distributed under the terms of the Oxford University Press, Standard Journals Publication Model (https://academic.oup.com/journals/pages/open_access/funder_policies/chorus/standard_publication_model)

Abstract

Background. The epidemiological advantage of Omicron variant is evidenced by its rapid spread and the ability to outcompete prior variants. Among Omicron sub-lineages, early outbreaks were dominated by BA.1 while BA.2 has gained dominance since February 2022. The relative pathogenicity and transmissibility of BA.1 and BA.2 have not been fully defined.

Methods. We compared viral loads and clinical signs in Syrian hamsters after infection with BA.1, BA.2, or D614G variant. A competitive transmission model and next generation sequencing were used to compare the relative transmission potential of BA.1 and BA.2.

Results. BA.1 and BA.2 caused no apparent clinical signs while D614G caused more than 10% weight loss. Higher viral loads were detected from the nasal washes, nasal turbinate and lungs of BA.1 than BA.2 inoculated hamsters. No aerosol transmission was observed for BA.1 or BA.2 under the experimental condition that D614G transmitted efficiently. BA.1 and BA.2 were able to transmit among hamsters via direct contact; however, BA.1 transmitted more efficiently than BA.2 under the competitive transmission model. No recombination was detected from direct contacts exposed simultaneously to BA.1 and BA.2.

Conclusions. Omicron BA.1 and BA.2 demonstrated attenuated pathogenicity and reduced transmission potential in hamsters when compared to early SARS-CoV-2 strains.

Keywords: SARS-CoV-2; Omicron; BA.1; BA.2; pathogenicity; transmission; Syrian hamsters.

ACCEPTED MANUSCRIPT

INTRODUCTION

Since the first report of severe acute respiratory syndrome coronavirus-2 (SARS-CoV-2) in December 2019, the ongoing COVID-19 pandemic has been sustained by the emergence of multiple variants of concern (VOC) that differ in their capacity to spread [1, 2], cause severe disease [3], or evade vaccine-induced immunity [4-8]. While the dynamics and the factors driving the emergence of VOC are not fully understood, it is anticipated that novel VOC will continue challenging our existing countermeasures [9-11] and diagnostic methods [12].

VOC Omicron (Pango lineage B.1.1.529) was first detected in Southern Africa in November 2021 and swept through the world within weeks [13]. Omicron has evolved into several major sub-lineages, with BA.1 as the initial dominant Omicron sub-lineage. The detection frequency of BA.2 has increased since early 2022 [14]. Omicron is genetically distinct from the prototype SARS-CoV-2 virus or other VOC that have previously spread regionally or globally. Compared to the prototype SARS-CoV-2 virus, Omicron VOC is characterized by more than 30 amino acid differences in the spike (S) glycoprotein and additional changes in the structural proteins (E, M, N), non-structural proteins (NSP3, 4, 5, 6, 12, 14), and accessory protein (ORF8)[14]. Detailed mutagenesis study using pseudoviruses has confirmed that multiple amino acid changes located at the receptor-binding domain (RBD) and the N-terminal domain (NTD) in Omicron may confer resistance to neutralizing monoclonal antibodies [15] and evasion to infection or vaccine-induced immunity [16, 17]. However, the effect of changes in RBD on viral attachment to human ACE2 has been under debate [18, 19].

Epidemiological data showed that infection with Omicron BA.1 was associated with reduced risk of hospitalization in South Africa where prior infections by SARS-CoV-2 were prevalent [20]. Experimental data showed that Omicron BA.1 exhibit reduced susceptibility to TMPRSS2 cleavage which reduced viral entry via fusion at plasma membrane [21]. Comparable replication of Delta and BA.1 was reported in human nasal epithelial cells [21], while BA.1 showed reduced replication in human lung ex vivo culture when compared to the

ACCEPTED MANUSCRIPT

prototype or Delta viruses [22]. It is not clear if the differential expression of TMPRSS2 in nasal and lung tissue or if additional host factors have affected BA.1 replication efficiency at upper and lower airway. Omicron BA.1 also caused attenuated replication in mice and Syrian hamsters when compared to other VOC, with reduced viral replication detected in the upper (mouse nasal turbinate) and lower respiratory tissues (mouse and hamster lungs) [23, 24].

While BA.2 is genetically related to BA.1, there are substantial differences in the S, M and N structural proteins, non-structural proteins (NSP1, 3, 4, 6, 13, 15) and accessory proteins (ORF3a and ORF6). Clinical severity and the risk of hospitalization were found to be comparable after BA.1 and BA.2 infections [25]. Prior vaccination and infection history may confound the transmission dynamics of VOC in the human population, and it is not clear if the increased detection frequency of BA.2 since February 2022 is due to an intrinsic fitness advantage of BA.2 over BA.1. Syrian hamsters have been reported to be an suitable animal model to study pathogenicity and transmissibility of SARS-CoV-2 [26-29]. Prototype SARS-CoV-2 replicates efficiently in the upper and lower respiratory tract and infected Syrian hamsters may lose 10-15% body weight [26-29]. In addition, SARS-CoV-2 may transmit efficiently among hamsters via multiple routes, among which transmission via aerosols was more efficient than via fomites [28, 29]. To study if there is an intrinsic fitness advantage of BA.2 over BA.1, we compared the pathogenicity and transmission potential of the two subvariants in Syrian hamsters.

METHODS

Cells and viruses. Vero E6 cells over-expressing transmembrane serine protease 2 (Vero-E6/TMPRSS2) were purchased from the Centre For AIDS Reagents (National Institute for Biological Standards and Control) and was maintained under condition as described previously [30, 31]. Omicron BA.1 (hCoV-19/Hong Kong/VM21044713_ HKUVOC0195P3/2021) [16], and BA.2 (hCoV-19/Hong Kong/VM22000135_ HKUVOC0588P2/2022) were isolated from the pooled nasopharyngeal and throat swabs of imported cases. Viruses were isolated and propagated 2 to 3 times in Vero-E6/TMPRSS2.

ACCEPTED MANUSCRIPT

The consensus sequences of the stock viruses were validated to be identical to the original clinical specimens by next generation sequencing.

Transmission experiments in Syrian hamsters. Male Syrian hamsters (AURA) at 4-8 weeks old were obtained from Laboratory Animal Services Centre, Chinese University of Hong Kong and from the Centre for Comparative Medicine Research, The University of Hong Kong. All experiments were performed at the BSL-3 core facility, LKS Faculty of Medicine, The University of Hong Kong. The study protocol has been approved by the Committee on the Use of Live Animals in Teaching and Research, The University of Hong Kong (CULATR # 5323-20).

To evaluate aerosol and contact transmission potential of D614G, Syrian hamsters were anesthetized with ketamine and xylazine and inoculated intranasally with 10^5 $TCID_{50}$ of SARS-CoV-2 in 80 µL PBS. On 1-day post-inoculation (dpi), one naïve hamster was exposed to an inoculated donor in an individually ventilated cage (IVC) for 8 hours (h) (eg. aerosol transmission model), with the animals separate by stainless-steel wires to prevent physical contact. After exposure, the D614G-inoculated donors were each co-housed with one naïve hamster for 24h (eg. from 32h to 56h post-inoculation) (eg. direct contact transmission model). To evaluate competitive transmissibility of BA.1 and BA.2 via aerosols, donors were anesthetized and separately inoculated with 1 x 10^5 $TCID_{50}$ of BA.1 or BA.2 in 80 µL PBS. Aerosol and direct contact transmission experiments were performed as described above, except that each naïve animal was simultaneously exposed to two donors inoculated with BA.1 and BA.2, respectively. The aerosol and contact transmission experiments were independently performed in duplicates or in triplicates. After exposure, all hamsters were single-housed in separate IVC cages until the end of the experiment. Weight changes and clinical signs were monitored daily. Nasal washes were harvested every other day from donors and exposed naïve hamsters. On 4 dpi, donors were euthanized to monitor viral replication in respiratory tissues. Nasal turbinate and lung (left) were homogenized in 1 mL PBS for viral load determination.

ACCEPTED MANUSCRIPT

Quantitative Real-time RT- PCR. Viral RNA was extracted using QIAamp Viral RNA Mini Kit (Qiagen). RNA was extracted from 70 µL of nasal washes and eluted with 60 µL elution buffer containing poly(A) carrier (AVE buffer) or from 140 µL of tissue homogenate and eluted with 60 µL AVE buffer. TaqManTM Fast Virus 1-Step Master Mix was used to determine N gene copy number with 4 µL of extracted RNA, following the conditions described previously [32].

Virus titration. Confluent Vero-E6/TMPRSS2 cells in 96-well culture plates were inoculated with 35 µL of serially half-log diluted samples in quadruplicate. Cytopathic effect of SARS-CoV-2 infection was observed under light microscope three days after infection, and the $TCID_{50}$ was calculated using the Reed-Muench method [33].

Histopathology and immunohistochemistry. Respiratory tissues, including head in sagittal cut, trachea, and right lung lobes were fixed in 10% neutral buffered formalin and were processed for paraffin embedding. For immunohistochemistry, SARS-CoV-2 viral proteins were detected using rabbit anti-N polyclonal antibody (#40143-T62, Sinobiological), mouse anti-N monoclonal antibody (#40143-MM05, Sinobiological), or rabbit anti-S1 monoclonal antibody (#99423, Cell Signaling) and counter-stained with hematoxylin. Images were captured using Nanozoomer slide scanner and viewed with NDP View software. To quantitatively compare the area with N protein detection, the percentage of positive pixels against the negative ones were calculated under 2.5x magnification using Aperio ImageScope (ver. 12.4.3).

Plaque reduction neutralization (PRNT) assay. Post-infection or post-exposure sera were heat-inactivated at 56°C for 30 min and were initially diluted 1:10 followed by serially 2-fold dilution using DMEM. Diluted sera were incubated with 30 plaque-forming units of SARS-CoV-2 for 1 h at 37 °C. The virus–serum mixtures were added to confluent Vero-E6/TMPRSS2 cells in 24-well plates and incubated 1 h at 37 °C. The inoculum was removed and the plates were overlaid with 0.5% agarose in culture medium and incubated for 3 days. The plates were fixed with 10% formalin and stained with 0.3% crystal violet to determine the number of plaques formed in the presence and absence of hamster sera. The serum

ACCEPTED MANUSCRIPT

dilution that resulted in > 50% reduction in the number of plaques was recorded as the $PRNT_{50}$ titers.

Next generation sequencing and data analysis. The virus genome was reverse transcribed with multiple gene-specific primers targeting different regions of the viral genome. The synthesized cDNA was then subjected to multiple overlapping 2-kb PCRs for full-genome amplification. PCR amplicons obtained from the same specimen were pooled and sequenced using iSeq 100 sequencing platform (Illumina). The sequencing library was prepared by Nextera DNA flex. The sequencing reads generated were trimmed by fastp [34] with adapter and quality filters and were mapped to a reference virus genome (Genbank accession: MN908947.3) by BWA-MEM2 (https://github.com/bwa-mem2/bwa- mem2). Potential PCR duplicates were identified and removed by samtools markdup (https://www.htslib.org/doc/samtools-markdup.html). The genome consensus sequence was generated by iVar with the PCR primer trimming protocol (minimum sequence depth >10 and minimum Q value of 30) [35]. The variants in the samples were called by bcftools v1.14 (https://samtools.github.io/bcftools/howtos/variant-calling.html). The number/frequency of different mutations were deduced from results of pysamstats (https://github.com/alimanfoo/pysamstats). The mutations frequencies at different genomic sites were curated and visualized using custom R scripts (available on Github: https://github.com/Leo-Poon-Lab/BA.1-BA.2-competitive-transmission-hamster).

Statistical analyses. Two-sided Mann-Whitney test was performed to compare the mean values of two groups, and Kruskal-Wallis test and Dunn's multiple comparisons post hoc test were used to compare the mean values of multiple groups. Spearman's rank correlation coefficient analysis was performed to evaluate the correlation between infectious virus load in oral swabs and nasal washes. Data were analyzed in Microsoft Excel for Mac, version 16.28 and GraphPad Prism version 8.4.1 for Windows (GraphPad Software, La Jolla, USA).

ACCEPTED MANUSCRIPT

RESULTS

Omicron BA.1 and BA.2 are less pathogenic in hamsters than the D614G variant. To compare the pathogenicity of Omicron BA.1 and BA.2 with an early D614G variant of SARS-CoV-2 virus (hCoV-19/Hong Kong/VM20109236/2020, EPI_ISL_2477019), hamsters were inoculated intranasally with 10^5 $TCID_{50}$ of viruses. While D614G-inoculated hamsters showed the maximal average weight loss of -13.00% on 6 dpi, hamsters inoculated with BA.1 or BA.2 showed minimal weight loss, with maximal average weight loss at -3.90% (1 dpi) and -4.55% (6 dpi), respectively (Figure 1A). On 2 dpi, comparable infectious viruses or viral RNA were detected from the nasal washes of BA.1- and D614G-inoculated hamsters, which were significantly higher than those detected from BA.2-inoculated hamsters (Figure 1B). On 4 dpi, the infectious viral loads in the nasal washes were comparable. In addition, there was a positive correlation between infectious viral load detected in the nasal washes and oral swabs (Spearman r= 0.592, p=0.046), although the virus titers detected in the oral swabs were around 2 logs lower than those detected in the nasal washes (Figure 1C). The mean infectious viral load detected in the nasal turbinate and lungs of BA.1-inoculated hamsters were higher than those of BA.2-inoculated hamsters, although the differences were not significant (Figure 1D).

Histopathological examination and immunohistochemistry were performed on nasal and lung tissues collected on 4 dpi. Since BA.1 and BA.2 differ by amino acid changes in the S and N protein, we compared the use of rabbit anti-N polyclonal antibody, mouse anti-N monoclonal antibody, and mouse anti-S monoclonal antibody in detecting BA.1 and BA.2 viral antigens in the lungs. Importantly, the mouse anti-S monoclonal antibody was able to detect BA.1 but not BA.2 viral antigen, highlighting the potential antigenic difference between the two S proteins. Rabbit anti-N polyclonal antibody that demonstrated best sensitivity for both BA.1 and BA.2 infected lungs was selected for subsequent analysis (Figure 2A). Viral antigens were detected in the nasal epithelial cells from BA.1 and BA.2 inoculated hamsters with minimal inflammation (Figure 2B). In the lungs, SARS-CoV-2 N protein was detected in focal bronchial epithelial cells and pneumocytes, accompanied with infiltration of

ACCEPTED MANUSCRIPT

mononuclear cells and lung consolidation. By calculating the percentage of positive pixels against the negative ones, higher percentages were detected in BA.1 than BA.2 infected nasal turbinates and lungs (Figure 2B), which is consistent with the detection of more infectious virus being detected in the nasal turbinates and lungs of BA.1 inoculated hamsters (Figure 1D). Overall, these results showed that BA.1 and BA.2 caused non-apparent clinical signs in Syrian hamsters when compared to the early SARS-CoV-2 D614G variant. BA.1 replicated more efficiently than BA.2 in both upper and lower respiratory tissues.

BA.1 and BA.2 cannot be transmitted in hamsters via aerosols. The D614G variant transmitted efficiently to exposed contact hamsters under the aerosol or direct contact transmission models (Figure 3A). Infectious virus and viral RNA were detected from the nasal washes of 2/2 aerosol contact hamsters at 1- and 3-days days post-exposure (dpe) and 2/2 direct contact hamsters at 1 dpe. The maximal weight loss (ranged from -6.5% to -14.8%) were detected from aerosol and direct contact hamsters on 7 to 8 dpe (Figure 3B). With the same experimental setting, we further evaluated the transmission potential of Omicron BA.1 and BA.2 under a competitive condition. Each naïve hamster was simultaneously exposed to two donor hamsters separately inoculated with 10^5 $TCID_{50}$ of BA.1 or BA.2. Under the experimental condition that support efficient aerosol transmission of D614G variant, we observed no transmission of BA.1 or BA.2. Specifically, no viral RNA was detected from the nasal washes (Figure 3C) and no seroconversion was detected from the aerosol contacts. Instead, transmission by direct contact was observed in 3/3 replicates, with infectious virus and viral RNA detected from the nasal washes of direct contact hamsters on 1 dpe (Figure 3C). No apparent weight loss was observed from the direct contact hamsters infected with BA.1/ BA.2 viruses (Figure 3D). Seroconversion was detected on 18 dpe, with all direct contact hamsters developing higher neutralizing antibody titers against BA.1 ($PRNT_{50}$ geometric mean titer at 179.3) than against BA.2 ($PRNT_{50}$ geometric mean titer at 57.7). Higher infectious viral loads, approximated by calculating the area under the curve (AUC), were shed by the D614G-exposed direct contacts (21.1 $\pm$ 0.8, mean $\pm$ SD AUC) than

ACCEPTED MANUSCRIPT

the BA.1/ BA.2-exposed direct contacts (18.4 ± 1.6, mean ± SD AUC) (Mann-Whitney test, p=0.20). Taken together, no aerosol transmission was observed for BA.1 and BA.2 viruses under the experimental condition that the D614G virus transmitted efficiently to naïve hamsters.

BA.1 transmits more efficiently than BA.2 in hamsters by direct contact. Next generation sequencing was performed to delineate the competitive transmission potential of BA.1 and BA.2 in direct contact hamsters. Using the SARS-CoV-2 isolate Wuhan-Hu-1 (GenBank: MN908947.3) as the reference, a total of 40 unique molecular markers were identified that differentiate BA.1 (N=14) and BA.2 (N=26) viruses after excluding mutations shared in common between BA.1 and BA.2. We first analyzed the nasal wash samples collected from BA.1 or BA.2 inoculated donors on 2 dpi (Figure 4A). High frequencies (≥ 91.73%) of BA.1 specific mutations and low frequencies (≤ 1%) of BA.2 specific mutations were detected from BA.1 inoculated donors. In contrast, high frequencies (≥ 95.66%) of BA.2 specific mutations and low frequencies (≤ 1%) of BA.1 specific mutations were detected from BA.2 inoculated donors. The NGS result suggests there was minimal secondary infection of BA.1 and BA.2 inoculated donors after co-housing for 32 h. In the nasal washes collected from direct contact hamsters on 1 and 3 dpe, we detected high frequencies (≥ 91.31 %) of BA.1 specific mutations and low frequencies (≤ 1.39 %) of BA.2 specific mutations, suggesting that the direct contact hamsters were preferentially infected by BA.1 virus.

Since BA.1 was the dominant virus transmitted under the competitive model, it is important to further confirm if BA.2 can transmit among hamsters via direct contact. After co-housing with donors inoculated with 10^5 $TCID_{50}$ of BA.1 or BA.2 on 1 dpi, infectious virus and viral RNA were detected from BA.1-exposed or BA.2-exposed contact hamsters on 1 dpe (Figure 5A, 5B). The maximal weight loss were recorded from BA.1-exposed hamsters (-1.41% and -1.58%) (Figure 5C) and BA.2-exposed hamsters (-1.75% and -2.46%) (Figure 5D) between 5 to 8 dpe. Higher viral loads were detected in the nasal washes of BA.1-

ACCEPTED MANUSCRIPT

exposed contacts (16.3 ± 0.9, mean ± SD AUC) than BA.2-exposed contacts (11.1 ± 0.6, mean ± SD AUC) (Mann-Whitney test, p=0.33). Taken together, the result demonstrates that both BA.1 and BA.2 are able to transmit among hamsters via direct contact; however, BA.1 transmits more efficiently than BA.2 in a competitive transmission model.

DISCUSSION

Since its first detection in November 2021, Omicron variant that is capable of evading neutralizing antibodies elicited after prior infections or vaccinations has rapidly replaced previously circulated SARS-CoV-2 VOC. In the present study, we evaluated the pathogenicity and transmission potential of Omicron sub-lineages BA.1 and BA.2 in Syrian hamsters. Compared to the early D614G virus that caused > 10% weight loss in inoculated hamsters, both BA.1 and BA.2 caused minimal weight changes and no apparent clinical signs in inoculated hamsters. Lower viral load was detected in the nasal washes of BA.2-inoculated hamsters than BA.1- or D614G- inoculated hamsters. Under the experimental conditions that D614G transmitted efficiently among Syrian hamsters via aerosol or direct contact transmission models, BA.1 and BA.2 was able to transmit among hamsters via direct contact alone. Furthermore, BA.1 transmitted more efficiently than BA.2 via direct contact under a competitive transmission model. Our result is consistent with previous studies that reported attenuated pathogenicity of BA.1 in hamsters when compared to previous SARS-CoV-2 strains [23], and that BA.2 is no more pathogenic than BA.1 in the Syrian hamster model [36]. The differential detection of BA.1 and BA.2 viral antigens by the anti-S monoclonal antibody highlights the potential antigenic differences in the S protein. Caution may be needed on the use of reagents to detect antigens of Omicron, and the use of polyclonal anti-N antibodies may provide less biased results across different SARS-CoV-2 variants.

Syrian hamsters have been a useful model to study SARS-CoV-2 transmission via multiple transmission routes [28, 29]. Interestingly, Omicron BA.1 and BA.2 lacked the ability to transmit in hamsters via aerosols under the experimental condition that the DD614G

ACCEPTED MANUSCRIPT

variant transmitted efficiently. The furin cleavage site at the S1/S2 junction was previously demonstrated to be required for SARS-CoV-2 transmission in the ferret model [37] and amino acid changes in proximity to the furin cleavage site may enhance viral fusion and pathogenicity [38]. Both omicron BA.1 and BA.2 contained N679K and P681H amino acid changes near the furin cleavage site. These changes were previously identified in other VOC and were associated with increased prevalence of Gamma sub-lineages in Brazil [39]. Omicron is different from previous SARS-CoV-2 in its reduced dependence on TMPRSS2 cleavage that facilitates fusion and entry at plasma membrane [21]. Instead, endosomal entry pathway is used by Omicron. In addition, by removing the furin cleavage site from SARS-CoV-2 or by introducing the furin cleavage site into SARS-CoV-1, it was shown that furin-cleavage site of S protein determines viral dependence on TMPRSS2 [40]. The furin-TMPRSS2 inter-dependence is also supported by the detection of variants with deletion in the furin cleavage site after passaging in Vero-E6 cells that lack TMPRSS2 [41]. Further studies are required to understand if the reduced TMPRSS2 dependence of Omicron has any effect on S1/S2 cleavage by furin in humans and in different animal models.

In a competitive transmission model, we observed that BA.1 transmitted more efficiently than BA.2 by direct contact. This may be due to less efficient viral replication of BA.2 in Syrian hamsters, as noted in viral load detected in nasal washes, nasal turbinates, and lungs. While both BA.1 and BA.2 may separately transmit to naïve direct contacts, it is interesting to note that NGS data suggest co-infection of BA.1 and BA.2 was infrequent under the competitive model. Specifically, high frequencies ($\geq$ 91.31 %) of BA.1 specific mutations and low frequencies ($\leq$ 1.39 %) of BA.2 specific mutations were detected in the nasal washes of direct contact hamsters on 1 and 3 dpe and no recombination of BA.1 and BA.2 was noted. Our experiments are limited by a small sample size, which may not fully recapitulate the viral dynamics in humans.

While animal models provide helpful insights on SARS-CoV-2 pathogenicity and transmissibility, the absence of aerosol transmission in hamsters appears to differ from what is epidemiologically observed in humans. This may limit the ability to extrapolate

ACCEPTED MANUSCRIPT

transmission data in hamsters to humans. However, the reduced pathogenicity of Omicron in Syrian hamsters is concordant to data observed in humans. It remains to be investigated if Omicron with multiple changes in the S protein has changed the ability to infect a wide range of mammalian species [42], although viral RNA of Omicron was recently detected in white-tailed deer [43].

In conclusion, Omicron BA.1 and BA.2 showed reduced pathogenicity and transmission potential when compared to prototype or D614G SARS-CoV-2 viruses in Syrian hamsters. Furthermore, BA.1 demonstrated transmission advantage over BA.2 via direct contact in hamsters. The reduced transmission potential of BA.1 and BA.2 in Syrian hamsters in comparison to previous SARS-CoV-2 provides a research opportunity to study host factors and virus-host interaction critical for SARS-CoV-2 transmission.

ACKNOWLEDGEMENTS

This study was supported by National Institute of Allergy and Infectious Diseases of the National Institutes of Health, USA (U01AI151810 and 75N93021C00016), RGC Theme-based Research Schemes, Hong Kong SAR, China (T11-712/19-N and T11-705/21-N).

ACCEPTED MANUSCRIPT

REFERENCES

1. Davies NG, Abbott S, Barnard RC, et al. Estimated transmissibility and impact of SARS-CoV-2 lineage B.1.1.7 in England. Science **2021**; 372.
2. Hart WS, Miller E, Andrews NJ, et al. Generation time of the alpha and delta SARS-CoV-2 variants: an epidemiological analysis. Lancet Infect Dis **2022**; 22:603-10.
3. Twohig KA, Nyberg T, Zaidi A, et al. Hospital admission and emergency care attendance risk for SARS-CoV-2 delta (B.1.617.2) compared with alpha (B.1.1.7) variants of concern: a cohort study. Lancet Infect Dis **2022**; 22:35-42.
4. Cao Y, Yisimayi A, Bai Y, et al. Humoral immune response to circulating SARS-CoV-2 variants elicited by inactivated and RBD-subunit vaccines. Cell Res **2021**; 31:732-41.
5. Cele S, Gazy I, Jackson L, et al. Escape of SARS-CoV-2 501Y.V2 from neutralization by convalescent plasma. Nature **2021**; 593:142-6.
6. Hoffmann M, Arora P, Gross R, et al. SARS-CoV-2 variants B.1.351 and P.1 escape from neutralizing antibodies. Cell **2021**; 184:2384-93 e12.
7. Planas D, Veyer D, Baidaliuk A, et al. Reduced sensitivity of SARS-CoV-2 variant Delta to antibody neutralization. Nature **2021**; 596:276-80.
8. Wu J, Nie J, Zhang L, et al. The antigenicity of SARS-CoV-2 Delta variants aggregated 10 high-frequency mutations in RBD has not changed sufficiently to replace the current vaccine strain. Signal Transduct Target Ther **2022**; 7:18.
9. Emary KRW, Golubchik T, Aley PK, et al. Efficacy of ChAdOx1 nCoV-19 (AZD1222) vaccine against SARS-CoV-2 variant of concern 202012/01 (B.1.1.7): an exploratory analysis of a randomised controlled trial. Lancet **2021**; 397:1351-62.
10. Eyre DW, Taylor D, Purver M, et al. Effect of Covid-19 Vaccination on Transmission of Alpha and Delta Variants. N Engl J Med **2022**; 386:744-56.
11. Madhi SA, Baillie V, Cutland CL, et al. Efficacy of the ChAdOx1 nCoV-19 Covid-19 Vaccine against the B.1.351 Variant. N Engl J Med **2021**; 384:1885-98.
12. Osorio NS, Correia-Neves M. Implication of SARS-CoV-2 evolution in the sensitivity of RT-qPCR diagnostic assays. Lancet Infect Dis **2021**; 21:166-7.
13. Viana R, Moyo S, Amoako DG, et al. Rapid epidemic expansion of the SARS-CoV-2 Omicron variant in southern Africa. Nature **2022**; 603:679-86.
14. Tsueng G, Mullen JL, Alkuzweny M, et al. Outbreak.info Research Library: A standardized, searchable platform to discover and explore COVID-19 resources. bioRxiv **2022**.
15. Liu L, Iketani S, Guo Y, et al. Striking antibody evasion manifested by the Omicron variant of SARS-CoV-2. Nature **2022**; 602:676-81.
16. Cheng SMS, Mok CKP, Leung YWY, et al. Neutralizing antibodies against the SARS-CoV-2 Omicron variant BA.1 following homologous and heterologous CoronaVac or BNT162b2 vaccination. Nat Med **2022**; 28:486-9.
17. Perez-Then E, Lucas C, Monteiro VS, et al. Neutralizing antibodies against the SARS-CoV-2 Delta and Omicron variants following heterologous CoronaVac plus BNT162b2 booster vaccination. Nat Med **2022**; 28:481-5.
18. Cameroni E, Bowen JE, Rosen LE, et al. Broadly neutralizing antibodies overcome SARS-CoV-2 Omicron antigenic shift. Nature **2022**; 602:664-70.
19. Han P, Li L, Liu S, et al. Receptor binding and complex structures of human ACE2 to spike RBD from omicron and delta SARS-CoV-2. Cell **2022**; 185:630-40 e10.
20. Wolter N, Jassat W, Walaza S, et al. Early assessment of the clinical severity of the SARS-CoV-2 omicron variant in South Africa: a data linkage study. Lancet **2022**; 399:437-46.
21. Meng B, Abdullahi A, Ferreira I, et al. Altered TMPRSS2 usage by SARS-CoV-2 Omicron impacts infectivity and fusogenicity. Nature **2022**; 603:706-14.
22. Hui KPY, Ho JCW, Cheung MC, et al. SARS-CoV-2 Omicron variant replication in human bronchus and lung ex vivo. Nature **2022**; 603:715-20.
23. Halfmann PJ, Iida S, Iwatsuki-Horimoto K, et al. SARS-CoV-2 Omicron virus causes attenuated disease in mice and hamsters. Nature **2022**; 603:687-92.

ACCEPTED MANUSCRIT

24. Shuai H, Chan JF, Hu B, et al. Attenuated replication and pathogenicity of SARS-CoV-2 B.1.1.529 Omicron. Nature **2022**; 603:693-9.
25. Fonager J, Bennedbaek M, Bager P, et al. Molecular epidemiology of the SARS-CoV-2 variant Omicron BA.2 sub-lineage in Denmark, 29 November 2021 to 2 January 2022. Euro Surveill **2022**; 27.
26. Chan JF, Zhang AJ, Yuan S, et al. Simulation of the Clinical and Pathological Manifestations of Coronavirus Disease 2019 (COVID-19) in a Golden Syrian Hamster Model: Implications for Disease Pathogenesis and Transmissibility. Clin Infect Dis **2020**; 71:2428-46.
27. Imai M, Iwatsuki-Horimoto K, Hatta M, et al. Syrian hamsters as a small animal model for SARS-CoV-2 infection and countermeasure development. Proc Natl Acad Sci U S A **2020**; 117:16587-95.
28. Port JR, Yinda CK, Owusu IO, et al. SARS-CoV-2 disease severity and transmission efficiency is increased for airborne compared to fomite exposure in Syrian hamsters. Nat Commun **2021**; 12:4985.
29. Sia SF, Yan LM, Chin AWH, et al. Pathogenesis and transmission of SARS-CoV-2 in golden hamsters. Nature **2020**; 583:834-8.
30. Matsuyama S, Nao N, Shirato K, et al. Enhanced isolation of SARS-CoV-2 by TMPRSS2-expressing cells. Proc Natl Acad Sci U S A **2020**; 117:7001-3.
31. Shirogane Y, Takeda M, Iwasaki M, et al. Efficient multiplication of human metapneumovirus in Vero cells expressing the transmembrane serine protease TMPRSS2. J Virol **2008**; 82:8942-6.
32. Chu DKW, Pan Y, Cheng SMS, et al. Molecular Diagnosis of a Novel Coronavirus (2019-nCoV) Causing an Outbreak of Pneumonia. Clin Chem **2020**; 66:549-55.
33. Reed LJ, Muench H. A simple method of estimating fifty percent endpoints. Am J Hyg **1938**; 27:493-7.
34. Chen S, Zhou Y, Chen Y, Gu J. fastp: an ultra-fast all-in-one FASTQ preprocessor. Bioinformatics **2018**; 34:i884-i90.
35. Grubaugh ND, Gangavarapu K, Quick J, et al. An amplicon-based sequencing framework for accurately measuring intrahost virus diversity using PrimalSeq and iVar. Genome Biol **2019**; 20:8.
36. Uraki R, Kiso M, Iida S, et al. Characterization and antiviral susceptibility of SARS-CoV-2 Omicron/BA.2. Nature **2022**.
37. Peacock TP, Goldhill DH, Zhou J, et al. The furin cleavage site in the SARS-CoV-2 spike protein is required for transmission in ferrets. Nat Microbiol **2021**; 6:899-909.
38. Saito A, Irie T, Suzuki R, et al. Enhanced fusogenicity and pathogenicity of SARS-CoV-2 Delta P681R mutation. Nature **2022**; 602:300-6.
39. Naveca FG, Nascimento V, Souza V, et al. Spread of Gamma (P.1) Sub-Lineages Carrying Spike Mutations Close to the Furin Cleavage Site and Deletions in the N-Terminal Domain Drives Ongoing Transmission of SARS-CoV-2 in Amazonas, Brazil. Microbiol Spectr **2022**; 10:e0236621.
40. Ou T, Mou H, Zhang L, Ojha A, Choe H, Farzan M. Hydroxychloroquine-mediated inhibition of SARS-CoV-2 entry is attenuated by TMPRSS2. PLoS Pathog **2021**; 17:e1009212.
41. Sasaki M, Uemura K, Sato A, et al. SARS-CoV-2 variants with mutations at the S1/S2 cleavage site are generated in vitro during propagation in TMPRSS2-deficient cells. PLoS Pathog **2021**; 17:e1009233.
42. Hobbs EC, Reid TJ. Animals and SARS-CoV-2: Species susceptibility and viral transmission in experimental and natural conditions, and the potential implications for community transmission. Transbound Emerg Dis **2021**; 68:1850-67.
43. Vandegrift KJ, Yon M, Surendran-Nair M, et al. Detection of SARS-CoV-2 Omicron variant (B.1.1.529) infection of white-tailed deer. bioRxiv **2022**.

ACCEPTED MANUSCRIPT

FIGURE LEGENDS

Figure 1. Pathogenicity of Omicron BA.1 and BA.2 in Syrian hamsters. Syrian hamsters were intranasally inoculated with BA.1(N=7), BA.2 (N=5) and D614G (N=8), respectively. *A*, Weight changes in inoculated do nor hamsters, mean ± SD are shown. *B*, Infectious viral load ($log_{10}TCID_{50}$/mL) and viral RNA (log_{10}RNA copies/mL) detected in nasal washes on 2, 4 dpi. *C*, Infectious viral load detected in oral swabs of inoculated donors on 2, 4 dpi. *D*, Infectious viral load detected in the nasal turbinates and lungs of inoculated donors on 4 dpi. Kruskal-Wallis test and Dunn's multiple comparisons were performed to compare weight changes and viral loads of BA.1, BA.2, and D614G inoculated hamsters at each time point (*A, B*). Mann-Whitney test was performed to compare viral loads of BA.1 and BA.2 inoculated hamsters (*C,D*). Spearman's rank correlation coefficient analysis (right) was performed to evaluate the correlation between infectious virus load in oral swabs (X axis) and nasal washes (Y axis). Experiments were independently performed 2-3 times. The limit of detection is shown with the dashed line.

Figure 2. **Detection of BA.1 and BA.2 viral antigens in the lungs and nasal cavity of inoculated Syrian hamsters by immunohistochemistry.** *A*, Lung tissues collected on 4 dpi from BA.1 or BA.2 inoculated hamsters were stained with rabbit anti-N polyclonal antibody, mouse anti-N monoclonal antibody, or mouse anti-S monoclonal antibody and counter stained with haematoxylin. *B*, Detection of N protein in nasal turbinates and lungs collected on 4 dpi of BA.1 (N=3) or BA.2 (N=3) inoculated hamsters using the rabbit anti-N polyclonal antibody and counterstained with haematoxylin. The percentage of positive pixels against the negative ones were calculated under 2.5x magnification using Aperio ImageScope (ver. 12.4.3).

Figure 3. Transmissibility of D614G, BA.1 and BA.2 in Syrian hamsters. Donors were intra-nasally inoculated with 10^5 $TCID_{50}$ of SARS-CoV-2 virus. On 1 dpi, naïve hamster was exposed to donors for 8h without physical contact (eg. aerosol transmission). Subsequently, donors were co-housed with another naïve hamster for 24h (eg. direct contact transmission).

ACCEPTED MANUSCRIPT

A, Infectious virus ($log_{10}TCID_{50}$/mL) and viral RNA (log_{10}RNA copies/ml) were detected in the nasal washes of D614G-exposed aerosol and direct contact hamsters. *B*, Weight changes of D614G-exposed aerosol contact and direct contact hamsters. *C*, Under a competitive transmission model, infectious virus ($log_{10}TCID_{50}$/mL) or viral RNA (log_{10}RNA copies/ml) were detected in the nasal washes of BA.1/BA.2-exposed direct contact hamsters. *D*, Weight changes of BA.1/BA.2-exposed aerosol contact and direct contact hamsters.

Figure 4. Detection of BA.1- and BA.2- specific markers by next generation sequencing. *A*, Detection frequency of BA.1- and BA.2- specific markers in the nasal washes of BA.1 or BA.2 inoculated donors on 1 dpi. *B*, Detection frequency of BA.1- and BA.2- specific markers in the nasal washes of exposed direct contact hamsters on 1 and 3 dpe. BA.1- and BA.2- specific markers differ from the prototype Wuhan-Hu-1 virus are shown. High allele frequency of BA.1-specific markers is shown in yellow while high allele frequency of BA.2 specific markers is shown in blue. Boxes with a cross denote regions with < 100 reads and were not included in the analysis.

Figure 5. Transmissibility of BA.1 and BA.2 via direct contact. *A*, Infectious virus ($log_{10}TCID_{50}$/mL) and viral RNA (log_{10}RNA copies/ml) were detected in the nasal washes of BA.1-exposed direct contact hamsters. *B*, Infectious virus ($log_{10}TCID_{50}$/mL) and viral RNA (log_{10}RNA copies/ml) were detected in the nasal washes of BA.2-exposed direct contact hamsters. *C*, Weight changes of BA.1-exposed direct contact hamsters. *D*, Weight changes of BA.2-exposed direct contact hamsters.

ACCEPTED MANUSCRIPT

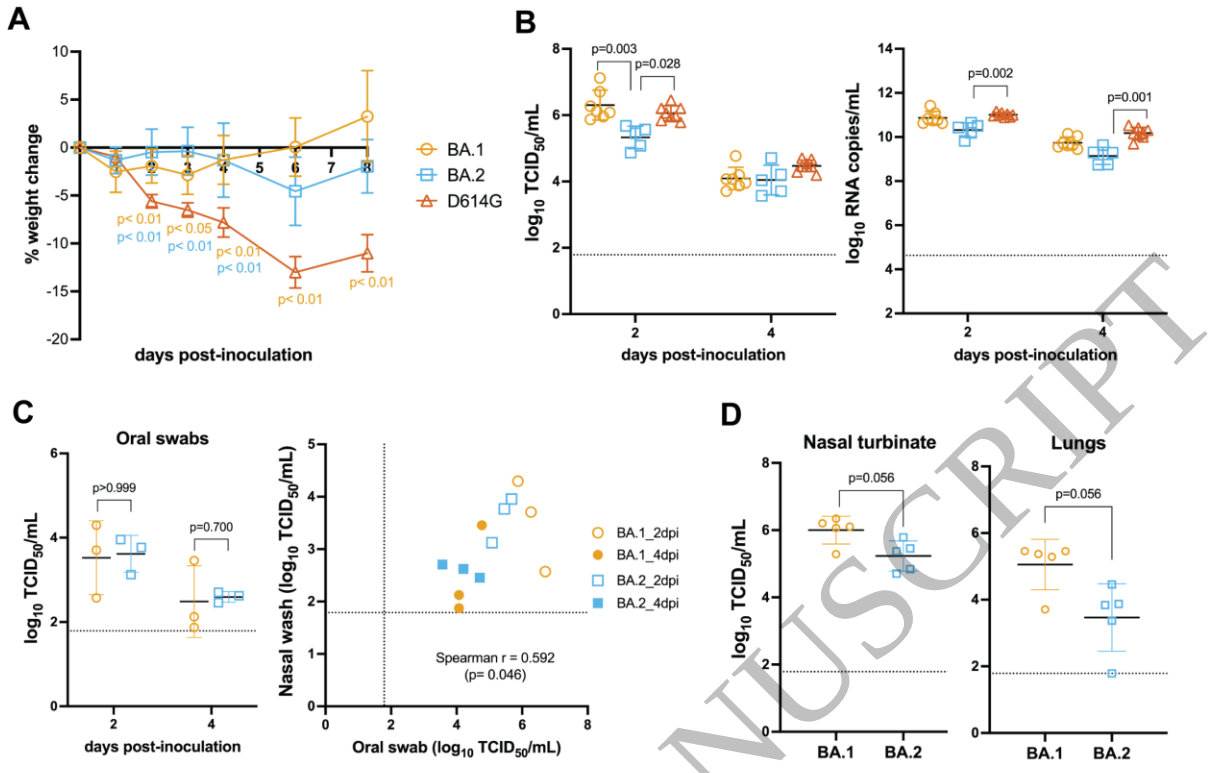

Figure 1
159x101 mm (.39 x DPI)

ACCEPTED MANUSCRIPT

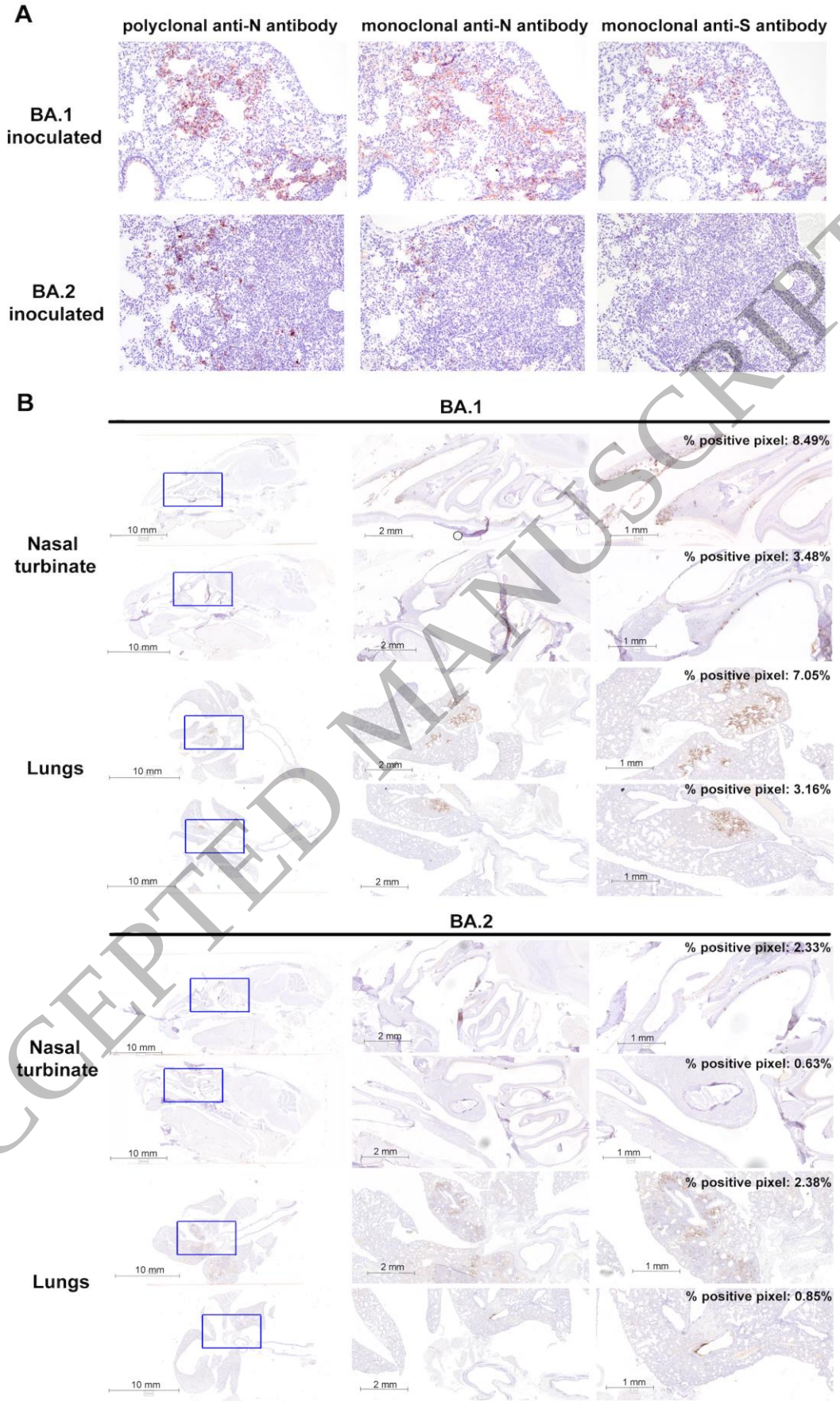

Figure 2
142x246 mm (.39 x DPI)

ACCEPTED MANUSCRIPT

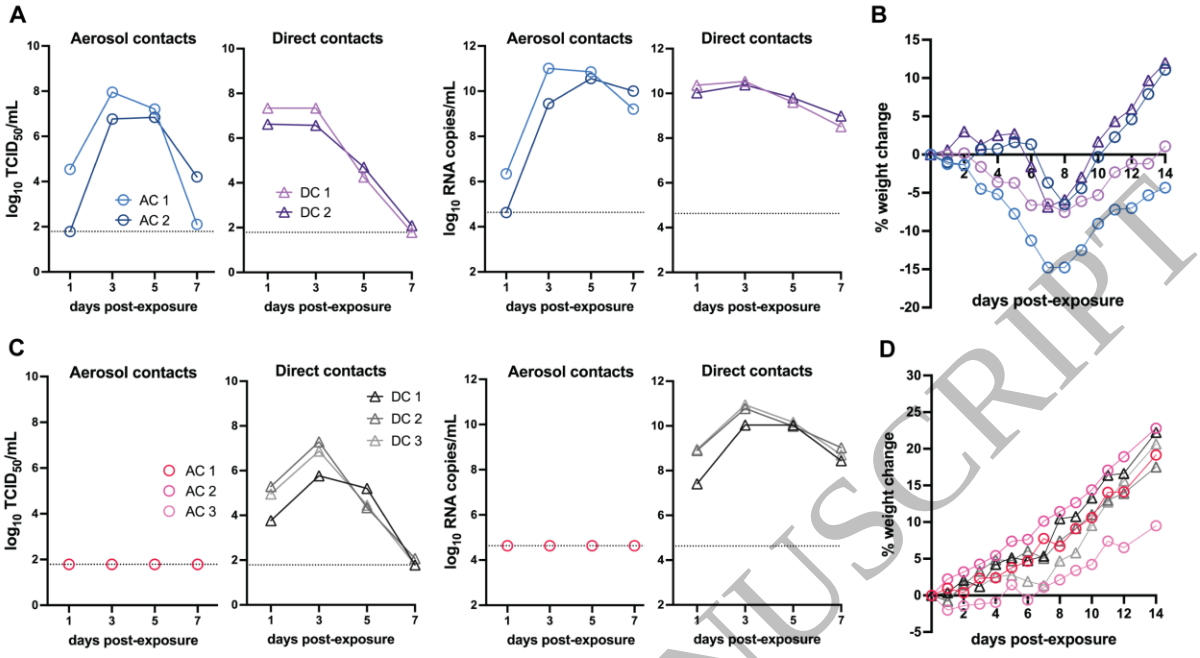

Figure 3
159x129 mm (.39 x DPI)

ACCEPTED MANUSCRIPT

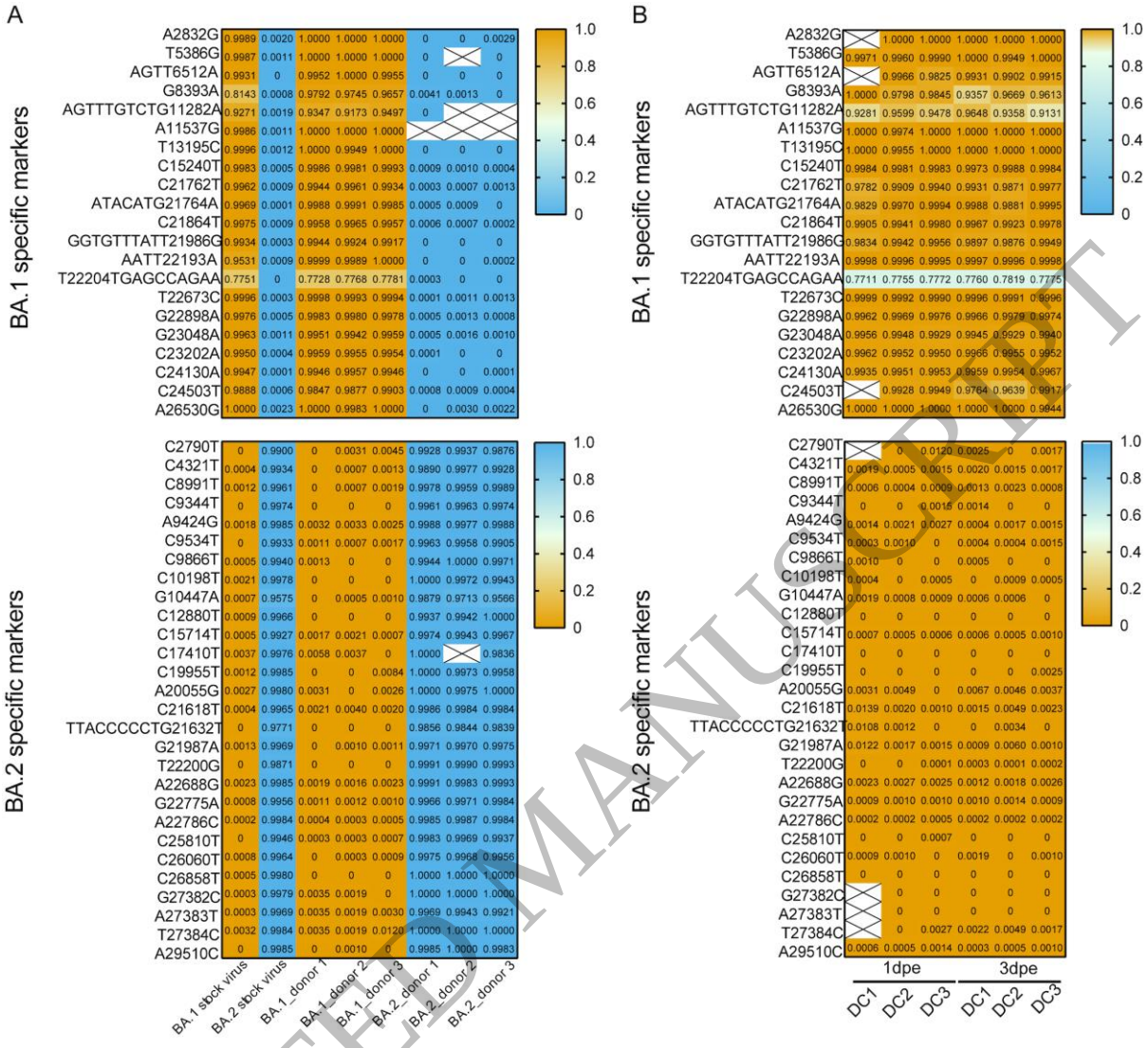

Figure 4
159x144 mm (.39 x DPI)

ACCEPTED MANUSCRIPT

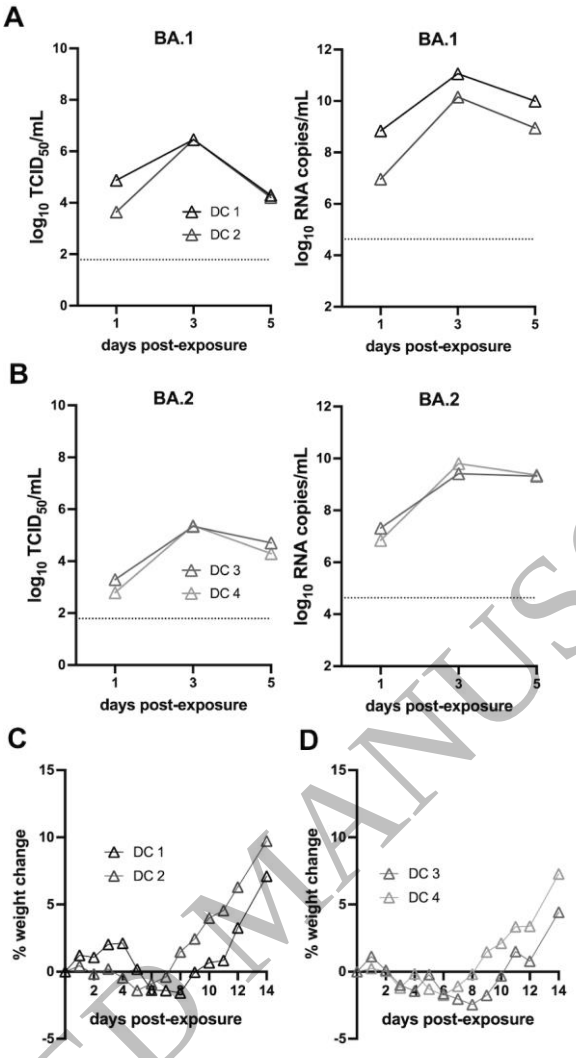

Figure 5
78x138 mm (.39 x DPI)

ACCEPTED MANUSCRIPT